Supplementary Material for "Extracting the number of type-B Goldstone modes and the dynamical critical exponent for a type of scale-invariant states"

Huan-Qiang Zhou,[1] Yan-Wei Dai,[1] Qian-Qian Shi,[1] Ian P. McCulloch,[2,3,1] and Murray T. Batchelor[4,1]

[1]Centre for Modern Physics, Chongqing University, Chongqing 400044, The People's Republic of China
[2] Department of Physics, National Tsing Hua University, Hsinchu 30013, Taiwan
[3]School of Mathematics and Physics, The University of Queensland, St. Lucia, QLD 4072, Australia
[4]Mathematical Sciences Institute, The Australian National University, Canberra ACT 2601, Australia

arXiv:2309.04953v2 [cond-mat.stat-mech] 30 Nov 2023

PACS numbers:

A. A subroutine to efficiently evaluate the block entanglement entropy $S_f(n)$

In order to extract the number of type-B GMs N_B, or equivalently, the fractal dimension d_f, from a finite-size scaling analysis of the block entanglement entropy $S_f(n)$, a subroutine is developed to efficiently evaluate the block entanglement entropy $S_f(n)$.

We assume that a ground state $|\psi\rangle$ in the iMPS representation is invariant under the two-site translation. Hence, it is represented by two tensors A_o and A_e, as shown in Fig. S1(a), where l and r are the bond indices: $l, r = 1, ..., \chi$, with χ being the bond dimension, and s is the physical index: $s = 1, ..., d$, with d being the dimension of the local Hilbert space.

The subroutine to efficiently evaluate the block entanglement entropy $S_f(n)$ consists of three steps, as shown in parts (b), (c) and (d) of Fig. S1: First, contract two tensors A_o and A_e to form one single tensor θ, reshape θ into a matrix G, labeled by the combined bond indices and the combined physical indices, perform a singular value decomposition for G, and truncate the physical indices, with a flow chart being shown in Fig. S2. Second, repeat the above process for a newly-formed tensor $A^{(1)}$ until the block size is reached, thus leading to a tensor Θ. Third, an approximation to the reduced density matrix ρ_n may be evaluated from the tensor Θ.

The subroutine is tested for the SU(2) spin-1/2 ferromagnetic states, with bond dimension $\chi = 50$. For comparison, the block entanglement entropy $S_f(n)$ takes the value 2.065418553 if no truncation is performed. Hence the subroutine yields a reliable result, with a relative error being less than 3.6×10^{-7}. See Table S1.

TABLE S1: The block entanglement entropy $S_f(n)$, with block size $n = 16$ and bond dimension $\chi = 50$, is evaluated for the SU(2) spin-1/2 ferromagnetic states. ϵ denotes a preset precision for performing repeated truncation.

ϵ	M_1	M_2	M_3	$S_f(n)$	relative error
10^{-3}	16	70	160	2.065417803	3.6×10^{-7}
10^{-4}	16	90	250	2.065418523	1.5×10^{-8}
10^{-5}	16	120	320	2.065418552	5.7×10^{-10}

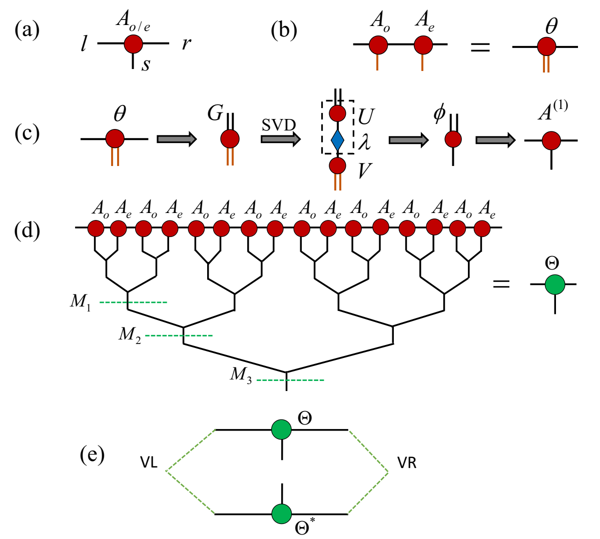

FIG. S1: (a) A single tensor $A_{o/e}$ in the iMPS representation. Here o/e refers to an odd/even site, l and r are the bond indices: $l, r = 1, ..., \chi$, with χ the bond dimension, and s the physical index: $s = 1, ..., d$, with d the dimension of the local Hilbert space. (b) Contraction of two tensors A_o and A_e to form one single tensor θ. (c) Reshape θ into a matrix G, labeled by the combined bond indices and the combined physical indices, perform a singular value decomposition for G, and truncate the physical indices to ensure that $|\lambda_M/\lambda_1| < \epsilon$, where $\lambda_1, \cdots, \lambda_M$ are the singular values, with M the number of states to be kept, and ϵ a preset precision. Afterwards, discard V and contract U and λ to form one single tensor ϕ and reshape it into one single tensor $A^{(1)}$. (d) Repeat this process until the block size is reached, thus leading to one single tensor Θ. (e) An approximation to the reduced density matrix for a block may be evaluated from Θ. Here we have chosen the block size $n = 16$ for illustration. Hence, a sequence of successive truncation consists of three different types of contractions, with M_1, M_2 and M_3 denoting the number of states to be kept after each successive truncation.

B. Finite block-size scaling of the entanglement entropy $S_f(n)$

The subroutine to efficiently evaluate the block entanglement entropy $S_f(n)$, described in Subsection A, is exploited to perform a finite block-size scaling analysis of the entanglement entropy $S_f(n)$ [S1, S2] for the three selected models – the spin-s Heisenberg ferromagnetic model, the SU(3) ferromagnetic model and the SO(4) spin-orbital model – in the context of the iDMRG algorithm [S3], with a fixed value of

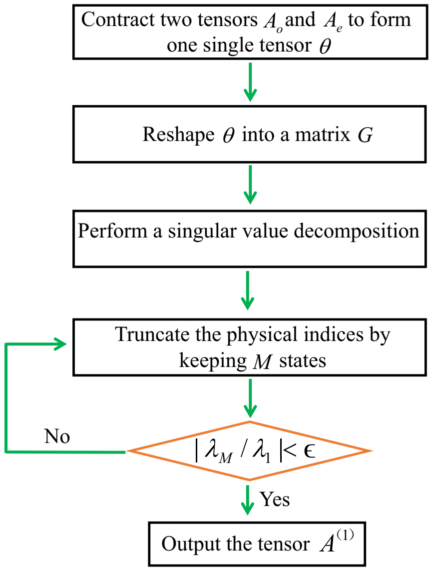

FIG. S2: A flow chart to contract two tensors Γ_A and Γ_B to form one single tensor θ, reshape θ into a matrix G, labeled by the combined bond indices and the combined physical indices, perform a singular value decomposition for G, and truncate the physical indices to ensure that $|\lambda_M/\lambda_1| < \epsilon$, where $\lambda_1, \ldots, \lambda_M$ are the singular values, with M being the number of states to be kept, and ϵ is a preset precision.

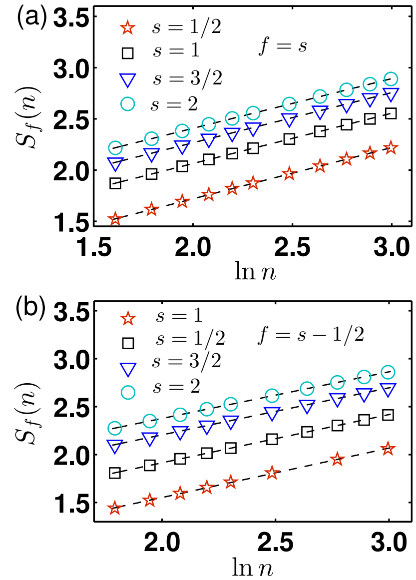

FIG. S3: The entanglement entropy $S_f(n)$ versus $\ln n$ for the SU(2) spin-s Heisenberg ferromagnetic model (1), with $s = 1/2, 1, 3/2$ and 2. We have chosen different fillings: (a) $f = s$ and (b) $f = s - 1/2$, with bond dimension $\chi = 160$.

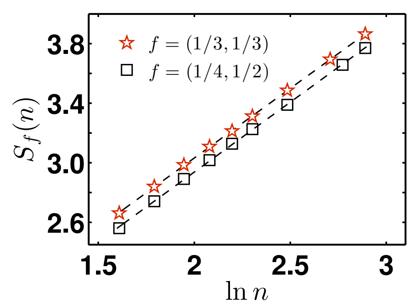

FIG. S4: The entanglement entropy $S_f(n)$ versus $\ln n$ for the SU(3) ferromagnetic model (4). The different fillings are as indicated, with bond dimension $\chi = 300$.

the bond dimension. A more detailed exposition on the extraction of the number of type-B GMs from different values of the bond dimension χ is outlined in Section D.

In Fig. S3, we plot the block entanglement entropy $S_f(n)$ versus $\ln n$ for the spin-s Heisenberg ferromagnetic model (3), with $s = 1/2, 1, 3/2$ and 2, as a simulation result of the U(1) iDMRG algorithm in the iMPS representation for different fillings f. For $f = s$, the number of type-B GMs is extracted to be $N_B = 1.002, 0.982, 0.9786$ and 0.97 for $s = 1/2, 1, 3/2$ and 2, respectively, where the block size ranges from $n = 5$ to $n = 20$. The relative error is less than 3%, compared to the exact value $N_B = 1$. For $f = s - 1/2$, the number of type-B GMs is extracted to be $N_B = 1.0298, 1.0052, 0.9804$ and 0.9722 for $s = 1/2, 1, 3/2$ and 2, respectively, with the block size ranging from $n = 6$ to $n = 20$. The relative error is less than 3% compared to the exact value $N_B = 1$.

In Fig. S4, we plot the block entanglement entropy $S_f(n)$ for the SU(3) ferromagnetic model (4), as a simulation result of the U(1) × U(1) iDMRG algorithm in the iMPS representation for $f = (1/3, 1/3)$ on the three-site unit cell and for $f = (1/4, 1/2)$ on the four-site unit cell. The best linear fit is exploited to estimate the number of type-B GMs $N_B = 1.8702$ for $f = (1/3, 1/3)$ and 1.8772 for (1/4, 1/2), with relative error less than 6.5%, compared to the exact value $N_B = 2$. The block size ranges from $n = 5$ to $n = 18$.

In Fig. S5, we plot the block entanglement entropy $S_f(n)$ versus $\ln n$ for the SO(4) spin-orbital model (5) with (a) $\zeta = 3/4$ and (b) $\zeta = \infty$, as a simulation result of the U(1) × U(1) iDMRG algorithm in the iMPS representation for $f = (1/2, 1/2)$ on the four-site unit cell and for $f = (5/12, 5/12)$ on the six-site unit cell. For $\zeta = 3/4$, the best linear fit is exploited to estimate the number of type-B GMs $N_B = 1.9104$ for $f = (1/2, 1/2)$ and 1.9352 for (5/12, 5/12), with relative error less than 4.5%, compared to the exact value $N_B = 2$. For $\zeta = \infty$, the best linear fit is exploited to estimate the number of type-B GMs $N_B = 1.9212$ for $f = (1/2, 1/2)$ and 1.9544 for (5/12, 5/12), with relative error less than 4%, compared to the exact value $N_B = 2$. The block size ranges from $n = 4$ to $n = 18$.

C. The dynamical critical exponent z from two types of correlation lengths

The correlation length ξ is defined as $\xi = 1/\ln|\Lambda_1/\Lambda_2|$ with Λ_1 and Λ_2 the largest and second largest eigenvalues of the transfer matrix E for a block consisting of n contiguous lattice

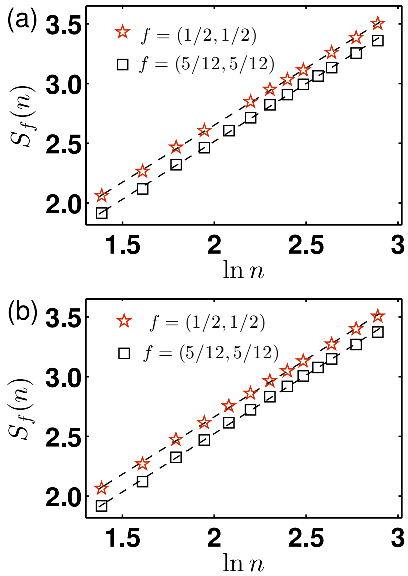

FIG. S5: The entanglement entropy $S_f(n)$ versus $\ln n$ for the SO(4) spin-orbital model (5) with (a) $\zeta = 3/4$ and (b) $\zeta = \infty$. The different fillings are as indicated, with bond dimension $\chi = 400$.

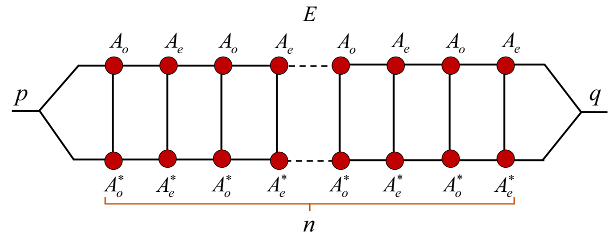

FIG. S6: A diagrammatical representation of the transfer matrix E, consisting of n contiguous lattice sites, with n even. Here $p = (p_1, \ldots, p_R)$ and $q = (q_1, \ldots, q_R)$ label the left and right bonds, with R the rank of a (semisimple) symmetry group G. The SSB pattern is from a symmetry group G to a residual symmetry group H: $G \to H$.

sites [S5], as schematically shown in Fig. S6. We exploit p and q to label the left and right bonds, where $p = (p_1, \ldots, p_R)$ and $q = (q_1, \ldots, q_R)$, with R being the rank of a (semisimple) symmetry group G. Here, the SSB pattern is from a symmetry group G to a residual symmetry group H: $G \to H$. Hence the entries of the transfer matrix E vanish unless $p = q$. That is, the transfer matrix E is in a block-diagonal form.

With this fact in mind, one may introduce two distinct types of correlation lengths, each of which in principle constitutes an infinite sequence. One type is $\xi_{u,q}$, defined as $\xi_{u,q} = 1/\ln(\Lambda_{1,q}/\Lambda_{2,q})$, which is restricted to a given sector labeled by q. Here all sectors are allowed, including the first sector, labelled by $q = (0, \ldots, 0)$. The other type is ξ_q ($q \neq (0, \ldots, 0)$), defined as $\xi_q = 1/\ln(\Lambda_{1,0}/\Lambda_{1,q})$, which involves two distinct sectors, labelled by $(0, \ldots, 0)$ and q. $\Lambda_{1,q}$ and $\Lambda_{2,q}$ denote the largest and second largest eigenvalues of the transfer matrix E in sector q. This is due to the fact that the spectrum of the transfer matrix E is split into different sectors. Actually, the correlation length ξ may be identified as one of the ξ_q's. Here we remark that, for a chosen value of the bond dimension χ, one is able to produce the correlation length $\xi_{u,q}(\chi)$ and the correlation length $\xi_q(\chi)$ from the iMPS representation.

Physically, the correlation length $\xi_{u,q}(\chi)$ in sector q, is *temporal*, because it essentially describes a time evolution, due to the fact that *only* one sector is involved. This amounts to stating that q is conserved. This is in contrast to the correlation length $\xi_q(\chi)$ which is *spatial*, since it involves different sectors such that a local spatial disturbance propagates across a given block, as far as the spread of information is concerned. Remarkably, for a scale-invariant state, one may expect that both the correlation length $\xi_{u,q}(\chi)$ and the correlation length $\xi_q(\chi)$ must scale with the bond dimension χ in an identical way, regardless of the values of q. More precisely, one may anticipate that the scaling relations of both the correlation length $\xi_{u,q}(\chi)$ and the correlation length $\xi_q(\chi)$ with the bond dimension χ in the iMPS representation do not depend on q. As a consequence, it is sufficient to consider $\xi_u(\chi)$ and $\xi(\chi)$, due to their practical q independence.

Hence it is necessary to take into account the dynamical critical exponent z, as it appears in the dispersion relation $\omega \sim k^z$. As such, we might speculate that there is a remarkable scaling relation between $\xi(\chi)$ and $\xi_u(\chi)$, of the form

$$\xi_u(\chi) \sim \xi^{1/z}(\chi). \tag{S1}$$

This offers an alternative means to extract the dynamical critical exponent z, which even holds for conformal field theory with $z = 1$, as a result of the Lorentz invariance. That is, there is no difference between the two choices, i.e., either $\xi(\chi)$ or $\xi_u(\chi)$, for conformally invariant states, if a scaling relation is concerned. In practice, this observation offers an alternative way to determine the correlation length ξ from simulation results of the iDMRG algorithm when a proper symmetry group is implemented. In contrast, this is not the case for scale-invariant states arising from SSB with type-B GMs, given they are not subject to the Lorentz invariance. Here, we remark that the correlation length $\xi_u(\chi)$ has been exploited in Ref. [S6] to study the scaling behavior of the entanglement entropy $S_f(\chi)$. Instead, the correlation length ξ has been adopted in Ref. [S7]. This explains the discrepancy between the scaling relations there.

As an illustration, we evaluate $\xi_{u,q}(\chi)$ for the spin-s Heisenberg ferromagnetic model (3), the SU(3) ferromagnetic model (4) and the SO(4) spin-orbital model (5). For our purpose, the iDMRG algorithm is the method of choice to simulate the models under investigation, since it is necessary to implement a proper symmetry group, i.e., the residual symmetry group H, to target a specific ground state [S4]. Specifically, the rank R is 1 for the spin-s Heisenberg ferromagnetic model, and the rank R is 2 for the SU(3) ferromagnetic model and the SO(4) spin-orbital model. Accordingly, the residual symmetry group U(1) has been implemented for the spin-s Heisenberg ferromagnetic model, and the residual symmetry group

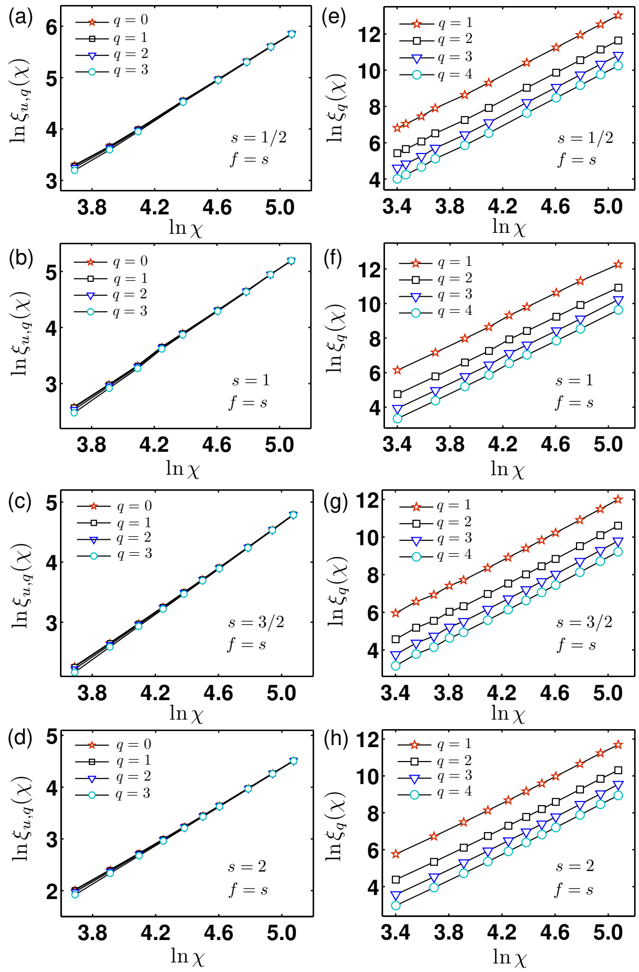

FIG. S7: The spin-s Heisenberg ferromagnetic model with filling $f = s$. (Left panels) Scaling relation between the correlation length $\xi_{u,q}(\chi)$ and bond dimension χ, with χ ranging from 40 to 160 and $q = 0, 1, 2, 3$: (a) $s = 1/2$; (b) $s = 1$; (c) $s = 3/2$; (d) $s = 2$. (Right panels) Scaling relation between the correlation length $\xi_q(\chi)$ in sector q and bond dimension χ, with χ ranging from 30 to 160 and $q = 1, 2, 3, 4$: (e) $s = 1/2$; (f) $s = 1$; (g) $s = 3/2$; (h) $s = 2$.

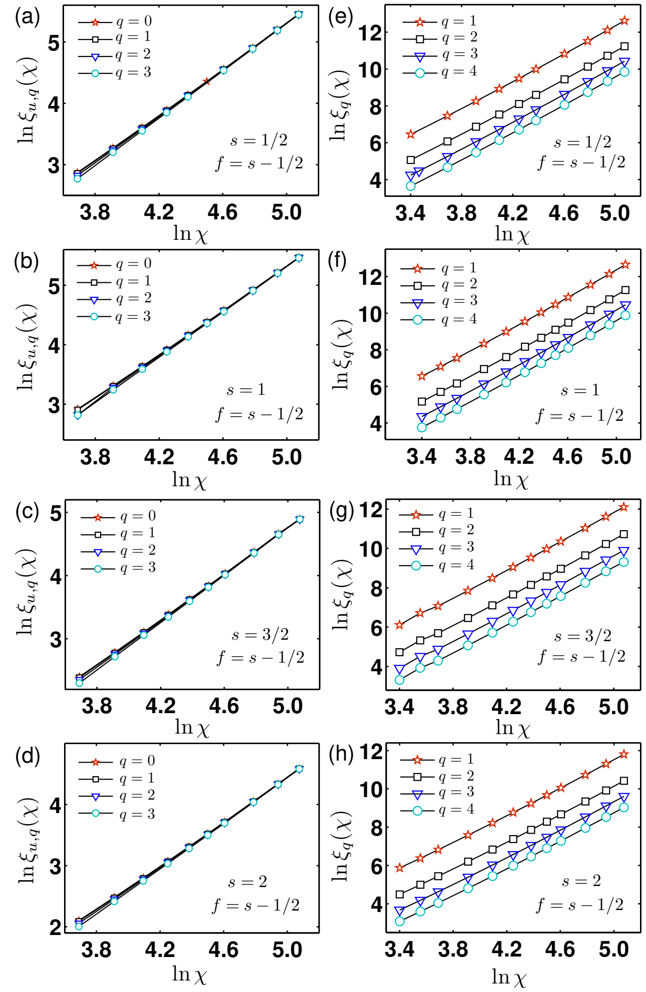

FIG. S8: The spin-s Heisenberg ferromagnetic model with filling $f = s - 1/2$. (Left panels) Scaling relation between the correlation length $\xi_{u,q}(\chi)$ and bond dimension χ, with χ ranging from 40 to 160 and $q = 0, 1, 2, 3$: (a) $s = 1/2$; (b) $s = 1$; (c) $s = 3/2$; (d) $s = 2$. (Right panels) Scaling relation between the correlation length $\xi_q(\chi)$ and bond dimension χ, with χ ranging from 30 to 160 and $q = 1, 2, 3, 4$: (e) $s = 1/2$; (f) $s = 1$; (g) $s = 3/2$; (h) $s = 2$.

U(1) × U(1) has been implemented for the SU(3) ferromagnetic model and the SO(4) spin-orbital model. In addition, we evaluate $\xi_q(\chi)$ for each of the three models. The dynamical critical exponent z can be extracted according to the scaling relation (S1) between $\xi_u(\chi)$ and $\xi(\chi)$.

1. The spin-s Heisenberg ferromagnetic model

For filling $f = s$, we plot the scaling of the correlation length $\xi_{u,q}(\chi)$ with bond dimension in Fig. S7(a)(b)(c)(d) and the scaling of the correlation length $\xi_q(\chi)$ with bond dimension in Fig. S7(e)(f)(g)(h), for the spin-s Heisenberg ferromagnetic model (3), with $s = 1/2, 1, 3/2$ and 2. The corresponding plots for filling $f = s - 1/2$ are shown in Fig. S8. Our numerical results confirm that the scaling relations for both correlation lengths $\xi_{u,q}(\chi)$ and $\xi_q(\chi)$, as follow from the iDMRG simulations in the iMPS representation, do not depend on q, within a reasonable error (less than 3.9%). As a consequence, one only needs to introduce the two correlation lengths $\xi_u(\chi)$ and $\xi(\chi)$, as far as their scaling relation is concerned.

For this same model, in Fig. S9 and Fig. S10, we plot the scaling relation between the correlation lengths $\xi_u(\chi)$ and $\xi(\chi)$ for $s = 1/2, 1, 3/2$ and 2, with different fillings $f = s$ and $f = s - 1/2$. The scaling relation (S1) is confirmed, regardless of our choice of sector q, to evaluate the correlation length $\xi_u(\chi)$, thus offering an alternative means to extract the dynamical critical exponent z. The best linear fits yield $z = 2$, with relative error less than 1%, compared to the exact value $z = 2$ from the conventional spin wave theory, as shown in Table S2 and Table S3.

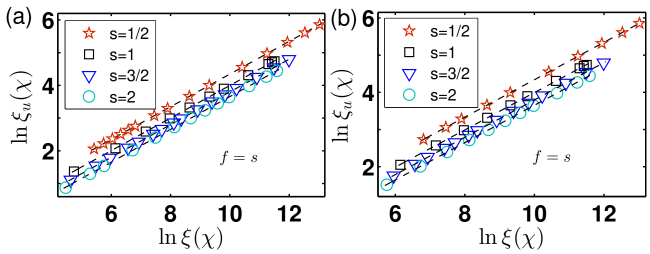

FIG. S9: Scaling relation between the correlation lengths $\xi_u(\chi)$ and $\xi(\chi)$ for the spin-s Heisenberg ferromagnetic model with $s = 1/2, 1, 3/2$ and 2 and filling $f = s$. Different sectors are labelled by q. (a) The sector $q = 0$, with bond dimension χ ranging from 20 to 160. (b) The sector $q = 1$, with bond dimension χ ranging from 30 to 160. Corresponding estimates for the scaling exponent are shown in Table S2.

TABLE S2: Estimates for the dynamical critical exponent z, compared to the exact value $z = 2$, for the spin-s Heisenberg ferromagnetic model, with filling $f = s$. Results for sectors $q = 0$ and $q = 1$ are shown.

Sector	s	1/2	1	3/2	2
$q = 0$		1.9988	1.9948	1.9992	2.0024
$q = 1$		2.0104	2.0052	2.0072	2.0076

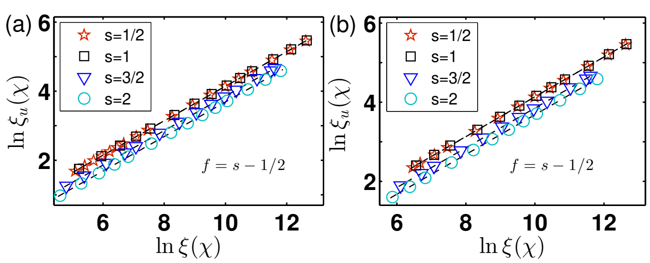

FIG. S10: Scaling relation between the correlation lengths $\xi_u(\chi)$ and $\xi(\chi)$ for the spin-s Heisenberg ferromagnetic model with $s = 1/2, 1, 3/2$ and 2 and filling $f = s - 1/2$. (a) The sector $q = 0$, with bond dimension χ ranging from 20 to 160. (b) The sector $q = 1$, with bond dimension χ ranging from 30 to 160. Corresponding estimates for the scaling exponent are shown in Table S3.

TABLE S3: Estimates for the dynamical critical exponent z, compared to the exact value $z = 2$, for the spin-s Heisenberg ferromagnetic model, with filling $f = s - 1/2$. Results for sectors $q = 0$ and $q = 1$ are shown.

Sector	s	1/2	1	3/2	2
$q = 0$		2.0004	1.9984	1.9972	2.0012
$q = 1$		2.0124	2.0096	2.006	2.0076

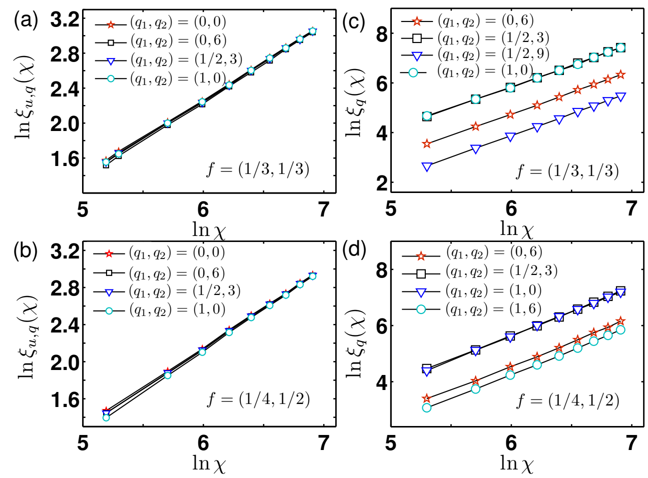

FIG. S11: The SU(3) ferromagnetic model. (Left panels) Scaling relation between the correlation length $\xi_{u,q}(\chi)$ and bond dimension χ, with χ ranging from 180 to 1000 and $(q_1, q_2) = (0, 0), (0, 6), (1/2, 3)$ and $(1, 0)$: (a) $f = (1/3, 1/3)$ and (b) $f = (1/4, 1/2)$. (Right panels) Scaling relation between the correlation length $\xi_q(\chi)$ and bond dimension χ, with χ ranging from 200 to 1000: (c) $f = (1/3, 1/3)$ and (d) $f = (1/4, 1/4)$. The sector values (q_1, q_2) are as indicated.

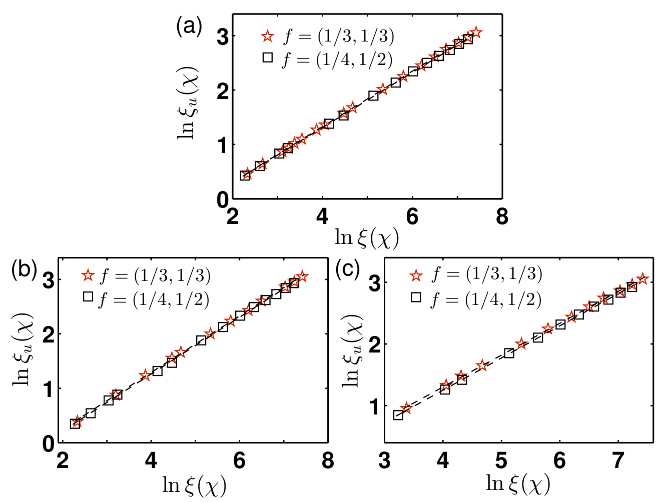

FIG. S12: Scaling relation between the correlation lengths $\xi_u(\chi)$ and $\xi(\chi)$ for the SU(3) ferromagnetic model for different sectors, with fillings $f = (1/3, 1/3)$ and $(1/4, 1/2)$. (a) The sector $(q_1, q_2) = (0, 0)$, with bond dimension χ ranging from 50 to 1000. (b) The sector $(q_1, q_2) = (1/2, 3)$, with bond dimension χ ranging from 50 to 1000. (c) The sector $(q_1, q_2) = (1, 0)$, with bond dimension χ ranging from 90 to 1000. Corresponding estimates for the scaling exponent are shown in Table S4.

2. *The* SU(3) *ferromagnetic model*

Turning to the SU(3) ferromagnetic model (4), for chosen fillings $f = (1/3, 1/3)$ and $f = (1/4, 1/2)$, we plot the scaling of the correlation length $\xi_{u,q}(\chi)$ with bond dimension in Fig. S11 (a)(b) and of correlation length $\xi_q(\chi)$ with bond dimension in Fig. S11(c)(d). Our numerical results confirm that

TABLE S4: The dynamical critical exponent estimates for the SU(3) ferromagnetic model in sector q with the indicated fillings.

Sector	f	$(1/3, 1/3)$	$(1/4, 1/2)$
$(q_1, q_2) = (0, 0)$		1.9589	1.9739
$(q_1, q_2) = (1/2, 3)$		1.9227	1.9135
$(q_1, q_2) = (1, 0)$		1.9346	1.9164

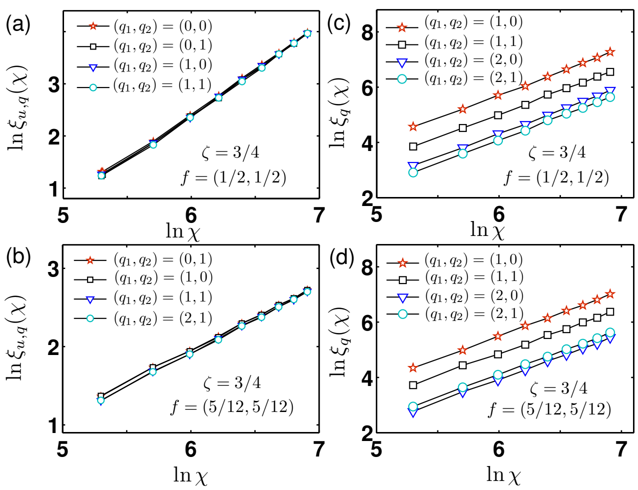

FIG. S13: The SO(4) spin-orbital model with $\zeta = 3/4$. (Left panels) Scaling relation between the correlation length $\xi_{u,q}(\chi)$ and bond dimension χ, with χ ranging from 200 to 1000 and indicated values for (q_1, q_2): (a) $f = (1/2, 1/2)$ and (b) $f = (5/12, 5/12)$. (Right panels) Scaling relation between the correlation length $\xi_q(\chi)$ and bond dimension χ, with χ ranging from 200 to 1000: (c) $f = (1/2, 1/2)$ and (d) $f = (5/12, 5/12)$.

the scaling relations for both correlation lengths with the bond dimension, as follows from the iDMRG simulations in the iMPS representation, do not depend on q, within a reasonable error (less than 4%). As a consequence, one only needs to introduce the two correlation lengths $\xi_u(\chi)$ and $\xi(\chi)$, as far as their scaling relation is concerned.

In Fig. S12, we plot the scaling relation between the correlation lengths $\xi_u(\chi)$ and $\xi(\chi)$ with fillings $f = (1/3, 1/3)$ and $(1/4, 1/2)$. The scaling relation (S1) is again confirmed, regardless of our choice of sector to evaluate the correlation length $\xi_u(\chi)$, thus offering an alternative means to extract the dynamical critical exponent z. The best linear fits yield $z = 2$, with a relative error less than 5%, compared to the exact value $z = 2$ from the conventional spin wave theory, as shown in Table S4.

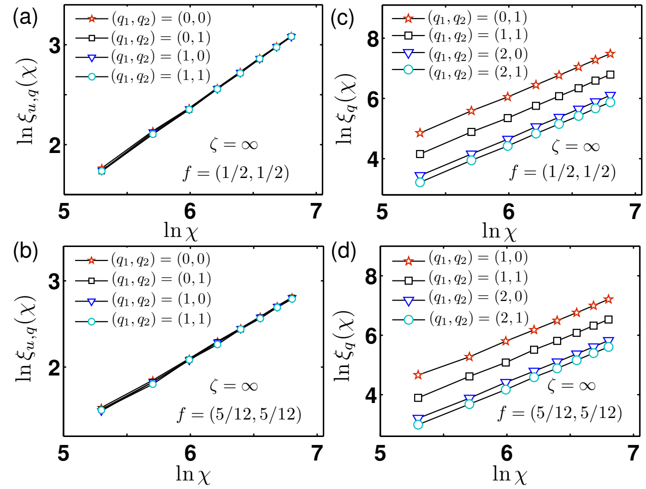

FIG. S14: The SO(4) spin-orbital model with $\zeta = \infty$. (Left panels) Scaling relation between the correlation length $\xi_{u,q}(\chi)$ and bond dimension χ, with χ ranging from 200 to 900 and indicated values for (q_1, q_2): (a) $f = (1/2, 1/2)$ and (b) $f = (5/12, 5/12)$. (Right panels) Scaling relation between the correlation length $\xi_q(\chi)$ and bond dimension χ, with χ ranging from 200 to 900: (c) $f = (1/2, 1/2)$ and (d) $f = (5/12, 5/12)$.

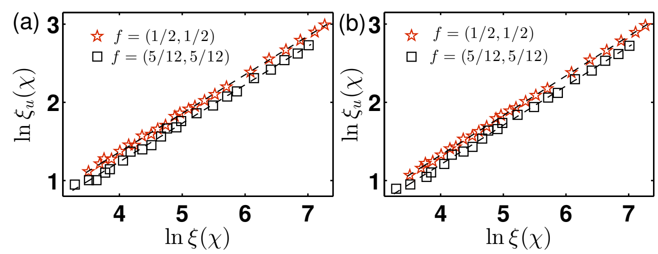

FIG. S15: Scaling relation between the correlation lengths $\xi_u(\chi)$ and $\xi(\chi)$ for the SO(4) spin-orbital model with $\zeta = 3/4$. (a) The sector $(q_1, q_2) = (0, 0)$ with bond dimension χ ranging from 100 to 1000. (b) The sector $(q_1, q_2) = (1, 0)$ with bond dimension χ ranging from 100 to 1000. The fillings are chosen to be $f = (1/2, 1/2)$ and $(5/12, 5/12)$. The corresponding estimates for the dynamical critical exponent z are given in Table S5.

3. *The* SO(4) *spin-orbital model*

For the SO(4) spin-orbital model (5) with $\zeta = 3/4$ and $\zeta = \infty$, and chosen fillings $f = (1/2, 1/2)$ and $(5/12, 5/12)$, we plot the scaling of the correlation length $\xi_{u,q}(\chi)$ with bond dimension in Fig. S13(a)(b) and S14(a)(b) and the correlation length $\xi_q(\chi)$ with the bond dimension χ in Fig. S13(c)(d) and S14(c)(d). Our numerical results for this model also confirm that the scaling relations for both correlation lengths $\xi_{u,q}(\chi)$ and $\xi_q(\chi)$ with bond dimension, as follow from the iDMRG simulations in the iMPS representation, do not depend on q, within a reasonable error (less than 3.5%). We thus only consider the two correlation lengths $\xi_u(\chi)$ and $\xi(\chi)$, as far as their scaling relation is concerned.

In Fig. S15 and Fig. S16, we plot the scaling relation be-

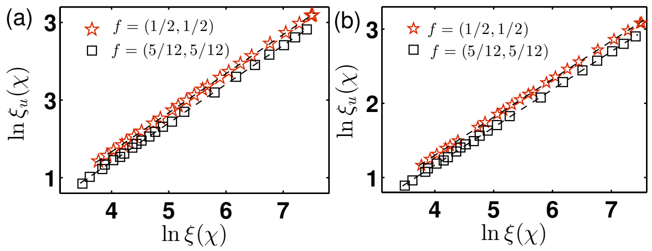

FIG. S16: Scaling relation between the correlation lengths $\xi_u(\chi)$ and $\xi(\chi)$ for the SO(4) spin-orbital model with $\zeta = \infty$. (a) The sector $(q_1, q_2) = (0, 0)$ with bond dimension χ ranging from 100 to 1000. (b) The sector $(q_1, q_2) = (1, 0)$ with bond dimension χ ranging from 100 to 1000. The fillings are chosen to be $f = (1/2, 1/2)$ and $(5/12, 5/12)$. The corresponding estimates for the dynamical critical exponent z are given in Table S6.

TABLE S5: Estimates of the dynamical critical exponent z for the SO(4) spin-orbital model with $\zeta = 3/4$ for sectors $(q_1, q_2) = (0, 0)$ and $(q_1, q_2) = (1, 0)$. The bond dimension ranges from 100 to 1000, with a relative error less than 2%, compared to the exact value $z = 2$. The fillings f are as indicated.

Sector	f	$(1/2, 1/2)$	$(5/12, 5/12)$
$(q_1, q_2) = (0, 0)$		2.0214	2.0288
$(q_1, q_2) = (1, 0)$		1.9728	1.99

tween the correlation lengths $\xi_u(\chi)$ and $\xi(\chi)$ with $\zeta = 3/4$ and $\zeta = \infty$, respectively. The scaling relation (S1) is again confirmed, regardless of our choice of a sector to evaluate the correlation length $\xi_u(\chi)$, thus offering an alternative means to extract the dynamical critical exponent z. In this case, the best linear fits yield $z = 2$, with the relative error less than 2% and 3%, compared to the exact value $z = 2$ from the conventional spin wave theory. The estimates are shown in Table S5 and Table S6.

D. The number of type-B GMs extracted from finite block-size scaling with increasing χ

As follows from a finite block-size scaling analysis of the entanglement entropy $S_f(n)$ [S1, S2] given in Eq. (1), the number of type-B GMs may be extracted from the iDMRG simulations [S3] for different values of the bond dimension χ, if a proper symmetry is implemented. In principle, one may perform an extrapolation to obtain an accurate estimate of the number of type-B GMs, as the bond dimension χ tends to infinity.

TABLE S6: Estimates of the dynamical critical exponent z for the SO(4) spin-orbital model with $\zeta = \infty$ for sectors $(q_1, q_2) = (0, 0)$ and $(q_1, q_2) = (1, 0)$. The bond dimension ranges from 100 to 1000, with a relative error less than 3%, compared to the exact value $z = 2$. The fillings f are as indicated.

Sector	f	$(1/2, 1/2)$	$(5/12, 5/12)$
$(q_1, q_2) = (0, 0)$		1.9853	1.9976
$(q_1, q_2) = (1, 0)$		1.9497	1.9585

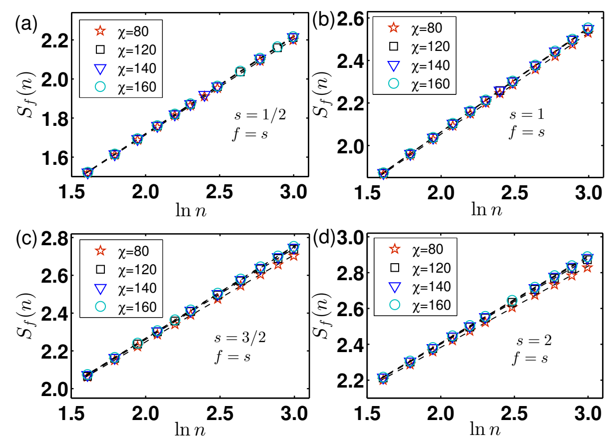

FIG. S17: The entanglement entropy $S_f(n)$ versus $\ln n$ for the SU(2) spin-s Heisenberg ferromagnetic model (3) with filling $f = s$, where (a) $s = 1/2$, (b) $s = 1$, (c) $s = 3/2$ and (d) $s = 2$. The bond dimensions are $\chi = 80, 120, 140$ and 160, with the block size ranging from $n = 5$ to $n = 20$.

1. *The* SU(2) *spin-s Heisenberg ferromagnetic model*

Fig. S17 shows a plot of the entanglement entropy $S_f(n)$ versus $\ln n$ for the SU(2) spin-s Heisenberg ferromagnetic model (3) with filling $f = s$ and different values of s. The

TABLE S7: Estimates for the number of type-B GMs N_B extracted from the finite block-size scaling of the entanglement entropy $S_f(n)$ for the SU(2) spin-s Heisenberg ferromagnetic model (3) with filling $f = s$ and bond dimensions $\chi = 80, 120, 140, 160$. The block size ranges from $n = 5$ to $n = 20$.

	χ	80	120	140	160
$s = 1/2$	N_B	0.9804	0.9946	0.9986	1.0002
$s = 1$	N_B	0.9534	0.9758	0.978	0.982
$s = 3/2$	N_B	0.9248	0.9668	0.9722	0.9786
$s = 2$	N_B	0.9054	0.9156	0.9632	0.97

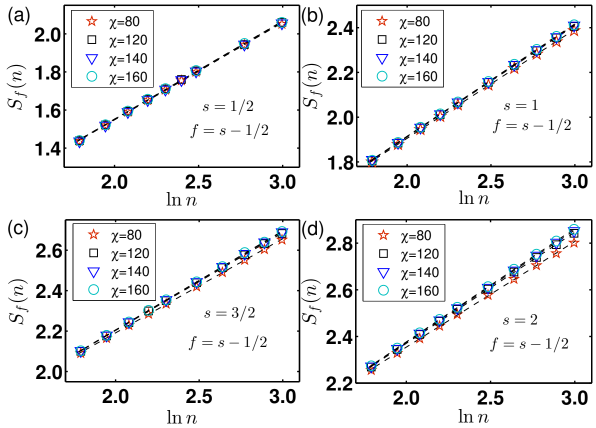

FIG. S18: The entanglement entropy $S_f(n)$ versus $\ln n$ for the SU(2) spin-s Heisenberg ferromagnetic model (3) with filling $f = s - 1/2$, where (a) $s = 1/2$, (b) $s = 1$, (c) $s = 3/2$ and (d) $s = 2$. The bond dimensions are $\chi = 80, 120, 140, 160$. The block size ranges from $n = 6$ to $n = 20$.

TABLE S8: Estimates for the number of type-B GMs N_B extracted from a finite block-size scaling of the entanglement entropy $S_f(n)$ for the SU(2) spin-s Heisenberg ferromagnetic model (3) with filling $f = s - 1/2$ and bond dimensions $\chi = 80, 120, 140, 160$. The block size ranges from $n = 6$ to $n = 20$.

	χ	80	120	140	160
$s = 1/2$	N_B	1.0214	1.0278	1.0288	1.0298
$s = 1$	N_B	0.9732	0.9962	0.999	1.0052
$s = 3/2$	N_B	0.931	0.9676	0.9756	0.9804
$s = 2$	N_B	0.9064	0.9526	0.9642	0.9722

best linear fit yields $N_B = 1$, with relative error less than 3%, with data shown in Table S7.

Fig. S18 shows a plot of the entanglement entropy $S_f(n)$ versus $\ln n$ for the SU(2) spin-s Heisenberg ferromagnetic model (3) with filling $f = s - 1/2$ and different values of s. The best linear fit yields $N_B = 1$, with a relative error less than 3%, as indicated in Table S8.

2. *The* SU(3) *ferromagnetic model*

Fig. S19 shows a plot of the entanglement entropy $S_f(n)$ versus $\ln n$ for the SU(3) ferromagnetic model (4) for different fillings. The best linear fit yields $N_B = 2$, with relative error less than 6.5%, as indicated in Table S9.

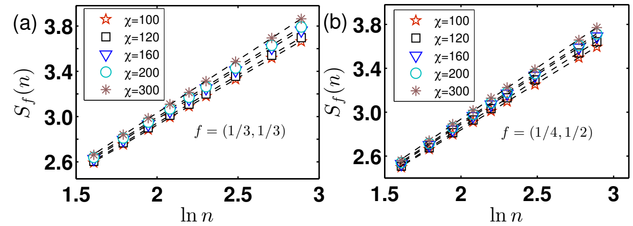

FIG. S19: The entanglement entropy $S_f(n)$ versus $\ln n$ for the SU(3) ferromagnetic model (4) for filling values (a) $f = (1/3, 1/3)$ and (b) $f = (1/4, 1/2)$. The bond dimensions are $\chi = 100, 120, 160, 200, 300$, with the block size ranging from $n = 5$ to $n = 18$.

TABLE S9: Estimates for the number of type-B GMs N_B extracted from the finite block-size scaling of the entanglement entropy $S_f(n)$ for the SU(3) ferromagnetic model (4) with fillings $f = (1/3, 1/3)$ and $f = (1/4, 1/2)$. The bond dimensions are $\chi = 100, 120, 160, 200, 300$, with the block size n ranging from $n = 5$ to $n = 18$.

	χ	100	120	160	200	300
$f = (1/3, 1/3)$	N_B	1.6686	1.6982	1.7732	1.791	1.8702
$f = (1/4, 1/2)$	N_B	1.704	1.771	1.8138	1.825	1.8772

3. *The* SO(4) *spin-orbital model*

Fig. S20 shows a plot of the entanglement entropy $S_f(n)$ versus $\ln n$ for the SO(4) spin-orbital model (5) with $\zeta = 3/4$, for different fillings. The best linear fit yields $N_B = 2$, with relative error less than 4.5%, as indicated in Table S10.

Fig. S21 shows a plot of the entanglement entropy $S_f(n)$ versus $\ln n$ for the SO(4) spin-orbital model (5) with $\zeta = \infty$, for different fillings. The best linear fit yields $N_B = 2$, with relative error less than 4%, as indicated in Table S11.

In summary, our results for the three illustrative models in-

TABLE S10: Estimates for the number of type-B GMs N_B extracted from the finite block-size scaling of the entanglement entropy $S_f(n)$ for the SO(4) spin-orbital model (5) with $\zeta = 3/4$. The fillings are $f = (1/2, 1/2)$ and $f = (5/12, 5/12)$, where the bond dimensions are $\chi = 60, 100, 200, 300, 400$, with block size ranging from $n = 4$ to $n = 18$.

	χ	60	100	200	300	400
$f = (1/2, 1/2)$	N_B	1.703	1.7302	1.7886	1.8516	1.9104
$f = (5/12, 5/12)$	N_B	1.7236	1.7466	1.8358	1.8906	1.9352

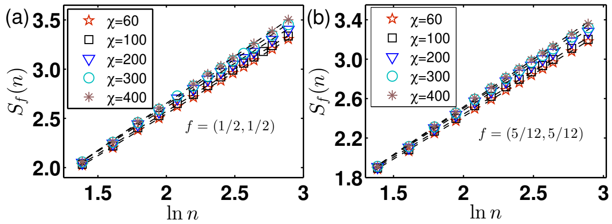

FIG. S20: The entanglement entropy $S_f(n)$ versus $\ln n$ for the SO(4) spin-orbital model (5) with $\zeta = 3/4$ for fillings (a) $f = (1/2, 1/2)$ and (b) $f = (5/12, 5/12)$. The bond dimensions are $\chi = 60, 100, 200, 300, 400$, with block size ranging from $n = 4$ to $n = 18$.

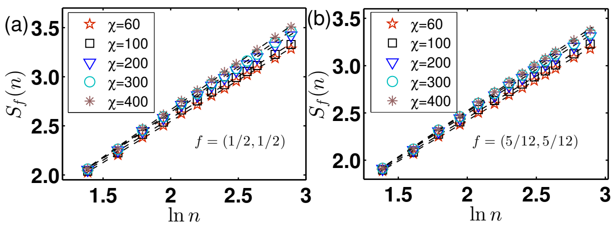

FIG. S21: The entanglement entropy $S_f(n)$ versus $\ln n$ for the SO(4) spin-orbital model (5) with $\zeta = \infty$. The fillings are (a) $f = (1/2, 1/2)$ and (b) $f = (5/12, 5/12)$, with bond dimensions $\chi = 60, 100, 200, 300, 400$, and block size ranging from $n = 4$ to $n = 18$.

dicate that the estimates for the number of type-B GMs N_B tend to saturate, as the bond dimension χ increases. As a consequence, we are led to conclude that the number of type-B GMs N_B may be reliably extracted from finite block-size scaling, as long as the bond dimension χ is large enough, within a reasonable accuracy.

TABLE S11: Estimates for the number of type-B GMs N_B extracted from the finite block-size scaling of the entanglement entropy $S_f(n)$ for the SO(4) spin-orbital model (5) with $\zeta = \infty$. The fillings are $f = (1/2, 1/2)$ and $f = (5/12, 5/12)$, with bond dimensions $\chi = 60, 100, 200, 300, 400$, and block size ranging from $n = 4$ to $n = 18$.

	χ	60	100	200	300	400
$f = (1/2, 1/2)$	N_B	1.6768	1.7058	1.813	1.8558	1.9212
$f = (5/12, 5/12)$	N_B	1.7232	1.7682	1.8662	1.9118	1.9544

[S1] Q.-Q. Shi, Y.-W. Dai, H.-Q. Zhou, and I. McCulloch, arXiv: 2201.01071 (2022).

[S2] H.-Q. Zhou, Q.-Q. Shi, I. McCulloch, and M. T. Batchelor, arXiv:2302.13126 (2023).

[S3] I. P. McCulloch, arXiv: 0804.2509 (2008); I.P. McCulloch, J. Stat. Mech. **2007**, P10014 (2007); F. Heidrich-Meisner, I. P. McCulloch, and A. K. Kolezhuk, Phys. Rev. B **81**, 179902 (2010); F. Zhan, J. Sabbatini, M. J. Davis, and I. P. McCulloch, Phys. Rev. A **90**, 023630 (2014).

[S4] All the relevant iDMRG codes, exploited in this work, may be downloaded from the website https://github.com/mptoolkit.

[S5] R. J. Baxter, Exactly-Solved Models in Statistical Mechanics (Academic Press, London, 1982).

[S6] P. Chen, Z.-L. Xue, I. P. McCulloch, M.-C. Chung, M. Cazalilla, and S. K. Yip, J. Stat. Mech. P10007 (2013).

[S7] Y.-W. Dai, Q.-Q Shi, H.-Q. Zhou, and I. McCulloch, arXiv: 2201.01434 (2022).